The Mechanical Significance of the Temporal Fasciae in *Macaca Fascicularis*: An Investigation Using Finite Element Analysis

NEIL CURTIS,[1]* ULRICH WITZEL,[2] LAURA FITTON,[3] PAUL O'HIGGINS,[3] AND MICHAEL FAGAN[1]

[1]Medical and Biological Engineering Research Group, Department of Engineering, University of Hull, Hull, United Kingdom

[2]Research Group of Biomechanics, Department of Engineering, University of Bochum, Bochum, Germany

[3]Functional Morphology and Evolution Unit, Hull-York Medical School, University of York, York, United Kingdom

ABSTRACT

Computational finite element analyses (FEAs) of the skull predict structural deformations under user specified loads and constraints, with results normally presented as stress and strain distributions over the skull's surface. The applied loads are generally a representation of the major adductor musculature, with the skull constrained at bite positions and at the articulating joints. However, virtually all analyses ignore potentially important anatomical structures, such as the fasciae that cover the temporalis muscle and attach onto the zygomatic arch. *In vivo* experimental studies have shown that removal of the temporal fasciae attachment onto the zygomatic arch in Cebus monkeys results in significant bone adaptation and remodeling in this region, suggesting the fasciae play an important role in stabilising the arch during biting. Here we investigate this potential stabilising role by carrying out FEAs of a macaque skull with and without temporal fasciae included. We explore the extent to which the zygomatic arch might be stabilized during biting by a synchronized tensioning of the temporal fasciae, acting to oppose masseteric contraction forces. According to our models, during temporalis muscle bulging the forces generated within the tensioned temporal fasciae are large enough to oppose the pull of the masseter. Further, a near bending-free state of equilibrium within the arch can be reached, even under forceful biting. We show that it is possible to eliminate the high strain gradients in and around the zygomatic arch that are present in past computational studies, with strains being more uniform in magnitude than previously thought. Anat Rec, 00:000–000, 2011. © 2011 Wiley-Liss, Inc.

Key words: primate; temporal fascia; masseter; temporalis; finite element analysis; skull; zygomatic arch

Grant sponsor: Biotechnology and Biological Sciences Research Council (BBSRC); Grant numbers: BB/E009204/1, BB/E014259/1.

*Correspondence to: Dr. Neil Curtis, Medical and Biological Engineering Research Group, Department of Engineering, University of Hull, Hull, HU6 7RX, United Kingdom. Fax: +44(0)1482 466664. E-mail: n.curtis@hull.ac.uk

Received 18 November 2010; Accepted 25 March 2011

DOI 10.1002/ar.21415

Published online in Wiley Online Library (wileyonlinelibrary.com).

INTRODUCTION

The skull houses and protects the brain and sensory organs, supports critical functions such as feeding and breathing, and provides a framework onto which muscles and other soft tissues attach and act. It is known that muscles are important in influencing skeletal growth and development (Moss and Salentijn, 1969), and perturbations of muscle action cause perturbations of growth that result in altered form (Moore, 1967). Thus, the skull is sculpted during growth and development through its interaction with applied loads, and forms a structure whose mechanical properties and geometry result in it being stiff enough to allow the muscles to function optimally (Currey, 2002, 2005; Preuschoft and Witzel, 2002).

Soft tissue structures other than the muscles are also present within the cranium, such as the dural septa (tentorium cerebelli, falx cerebri, and falx cerebelli) and septal cartilage. It has been suggested that these structures may play a functional role and thereby be important to craniofacial form. The dural septa run transversely and sagittally through the cranial cavity, and it has been argued they could transmit the postcervical neck muscle forces through the cranium (Shira, 1981). The septal cartilage, which stretches from the perpendicular plate of the ethmoid to the external nose, may play some role in transmitting and dampening masticatory loads (Al Dayeh et al., 2009). Another potentially important external structure is the deep temporal fascia, which originates from the periosteum of the superior temporal line and attaches strongly to the superior border and lateral surface of the zygomatic arch (Eisenberg and Brodie, 1965; Wormald and Alun-Jones, 1991; Oxnard and Franklin, 2008). It has been suggested that the fasciae aid the zygomatic arch in resisting the tensions of the masseter muscle, which may be large during forceful biting (Eisenberg and Brodie, 1965).

When the zygomatic arch is fractured, it is rarely pulled down by masseter muscle contraction. Instead, isolated zygomatic arch fractures in humans often result in a characteristic "V-shaped" displacement of the bones, composed of three separate fracture lines and two bone fragments (Fujii and Yamashiro, 1983; Werner et al., 2002; Turan et al., 2004; Rodriguez-Vegas et al., 2004). The two bone fragments rotate medially from the outer fracture lines like a hinge, shifting horizontally toward the temporal fossa along the third, middle fracture line. This medial displacement of the fractured bones may be a result of misalignment between the forces of the temporal fascia and the forces of the masseter muscle. This misalignment could produce a medially directed resultant force (as presented by Witzel et al., 2004: Figs. 5–7), that causes the zygomatic arch to respond as a compression-resistant vault (also see Witzel et al., 2011). It is interesting that animals such as moles, shrews, hedgehogs, anteaters and sloths present incomplete zygomatic arches but still have well-developed masseter muscles (Brodie, 1952). This may be attributable to a more vertical alignment between the temporal fasciae and the masseter muscle.

More evidence that the fasciae oppose the pull of the masseter muscle is presented in a case study by Holmes (1912). Here, a patient with congenital absence of the anterior part of both the arch and the temporal muscle is described. Interestingly, a narrow tendinous band was observed that bridged the gap in the arch and onto which the temporal and masseteric fascia were both attached. No depression of the incomplete arch was noted during biting. Perhaps, the strongest evidence that the temporal fasciae aid in resisting the tensions of the masseter muscle is provided by Eisenberg and Brodie (1965). In their study of Cebus monkeys, they found that disconnection of the fasciae from the zygomatic arch caused the arch to remodel 4 mm lower and 2 mm closer to the midline. The distributions of deposition and resorption indicated that the marrow spaces and zygomaticotemporal suture drifted in the direction of the unopposed pull of the masseter.

Computational techniques such as finite element analysis are popular for exploring the mechanical function of skulls (e.g., Ross et al., 2005; Kupczik et al., 2007, 2009; Strait et al., 2007, 2009; Wroe et al., 2007, 2010; Curtis et al., 2008; Dumont et al., 2010; Wang et al., 2010), but it is rare that the temporal fasciae are taken into account (Witzel et al., 2011). As a result most analyses, particularly in skulls with relatively weak zygomatic arches, predict large inferior bending of the arch producing elevated levels of strain and high strain gradients across the skull. Here, we investigate the influence of including the temporal fasciae in finite element analyses (FEAs), and assess whether or not it is possible for the fasciae to aid the zygomatic arch in resisting the tensions of the masseter muscle in macaques.

A combination of two- and three-dimensional finite element models were developed that incorporate the deep temporal fascia, whose details of attachment in standard descriptions were confirmed via dissection. By varying the restraining properties of the deep fascia, we assess the impact of their inclusion on zygomatic arch strains. In doing so, we also investigate the possibility that temporalis muscle bulging, which occurs when the muscle contracts, may synchronise tension within the fasciae with the contraction of the masseter muscle, thus further stabilising the zygomatic arch. This theory was first discussed by Witzel et al. (2004), who put forward the opinion that the tensioned fascia would counter the pull of the masseter, and possibly eliminate bending within the arch. If such a mechanism is mechanically plausible, it would provide a basis for reconsidering the role of the temporalis fascia during biting with a view to improving the loading of future functional simulations.

MATERIALS AND METHODS

Dissection and Materials Testing

Dissection was undertaken of a subadult *Macaca fascicularis* (unknown sex: MAC-10, Hull-York Medical School, York, UK) and an adult female macaque (MAC-145, Hull-York Medical School, York, UK) to confirm the structure, relations and attachments of the fascial layers over the temporalis muscle. These individuals had been curated for ~20 years in various storage media; at various times alcohol, formalin, water, and other unknown agents. It is likely that these have affected the mechanical properties of the fascia. As such this material is rendered unsuitable for reliable materials testing. Therefore, the material properties of fascial samples from a lightly and recently embalmed adult male human cadaver were determined

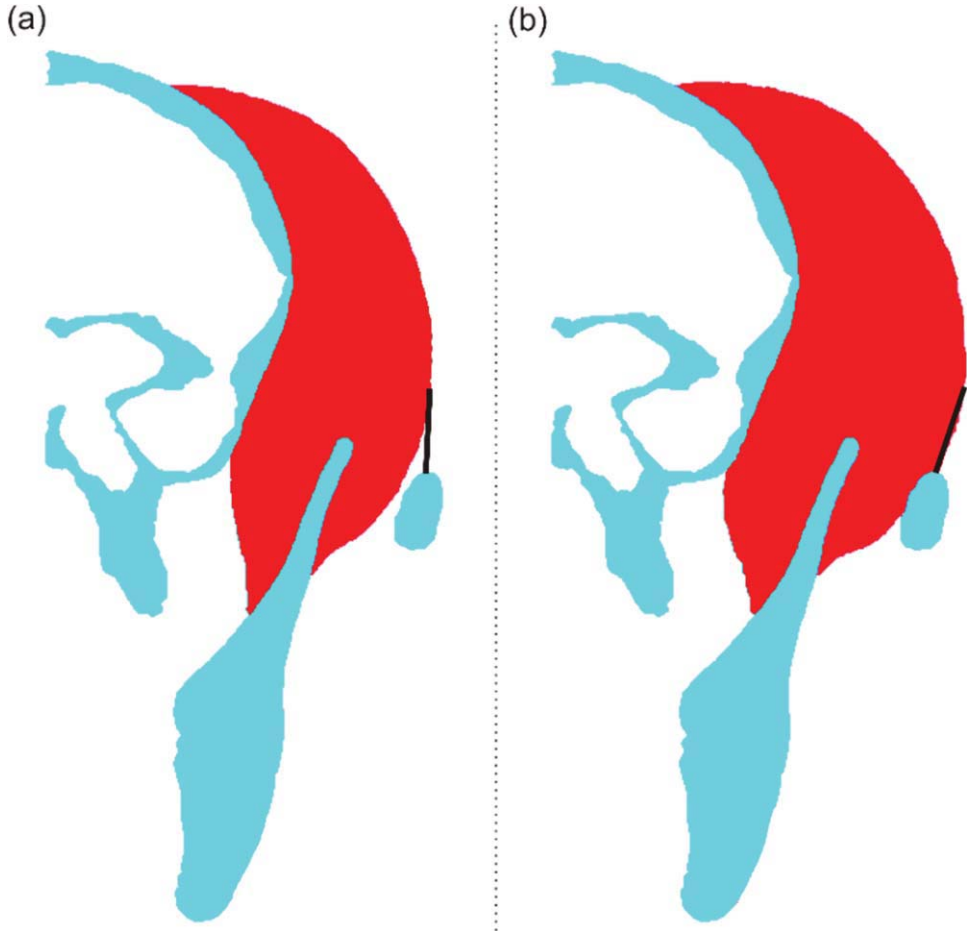

Fig. 1. 2D finite element model representing a cross-section of the left side of a macaque cranium and mandible. Blue = bone; red = temporalis muscle; black line = end of the fascia. **a**: no muscle bulging and **b**: muscle bulging (three times exaggerated).

experimentally to obtain working approximations to inform modeling. The fascial layers were separated and a patch of the most superficial layer (superficial temporal fascia) and a patch of the deeper layer (deep temporal fascia) were removed. These were submitted to materials testing using a dynamic materials analyser (DMA Q800, TA Instruments, Crawley, UK). Rectangular samples of approximately 10 mm × 5 mm were prepared and clamped into the dynamic materials analyser (DMA) in such a way as they were loaded in the direction of major fiber orientation. The samples were subjected to a tensile test until failure under a constant load rate of 2 N/min. In total, four samples of the superficial layer and four samples of the deeper layer were tested (eight samples in total).

Finite Element Analysis

A two-dimensional FEA was performed to estimate the increase in length of the outer surface of the temporalis muscle as it bulges during contraction. Assuming the deep temporal fascia is closely applied (as it appears to be in dissections) over the temporalis muscle, its extension can be inferred.

Using micro-CT data of an adult male *Macaca fascicularis* skull (lacking M3; MAC-14, Hull-York Medical School, York, UK) scanned at the University of Hull for a previous study (Kupczik et al., 2007), a representative cross-section was taken, approximately midway along the length of the arch, that included the temporal region with zygomatic arch and the mandible. The cross-section was edited to leave only the left side of the skull and mandible. Within image editing and segmentation software (AVIZO 5, VSG) a corresponding section through the temporalis muscle was incorporated, originating on the cranium and inserting on the mandible. The two-dimensional (2D) image was then converted into a triangular mesh in preparation for a finite element analysis. The meshed geometry was imported into commercially available FEA software (ANSYS version 12, ANSYS), and all muscle and bone structures were defined with six or eight noded (plane strain) second-order elements. Bone was specified with a Young's modulus of 17 GPa and a Poisson's ratio of 0.3 (consistent with direct measurements and within the ranges applied by others; Strait et al., 2005; Witzel and Preuschoft, 2005; Dumont et al., 2009; Wang et al., 2010), and the temporalis muscle with a Young's modulus of 10 MPa and a Poisson's ratio of 0.3. Notional thermal expansion properties were additionally assigned to the muscle elements so that their expansion (bulging) could be

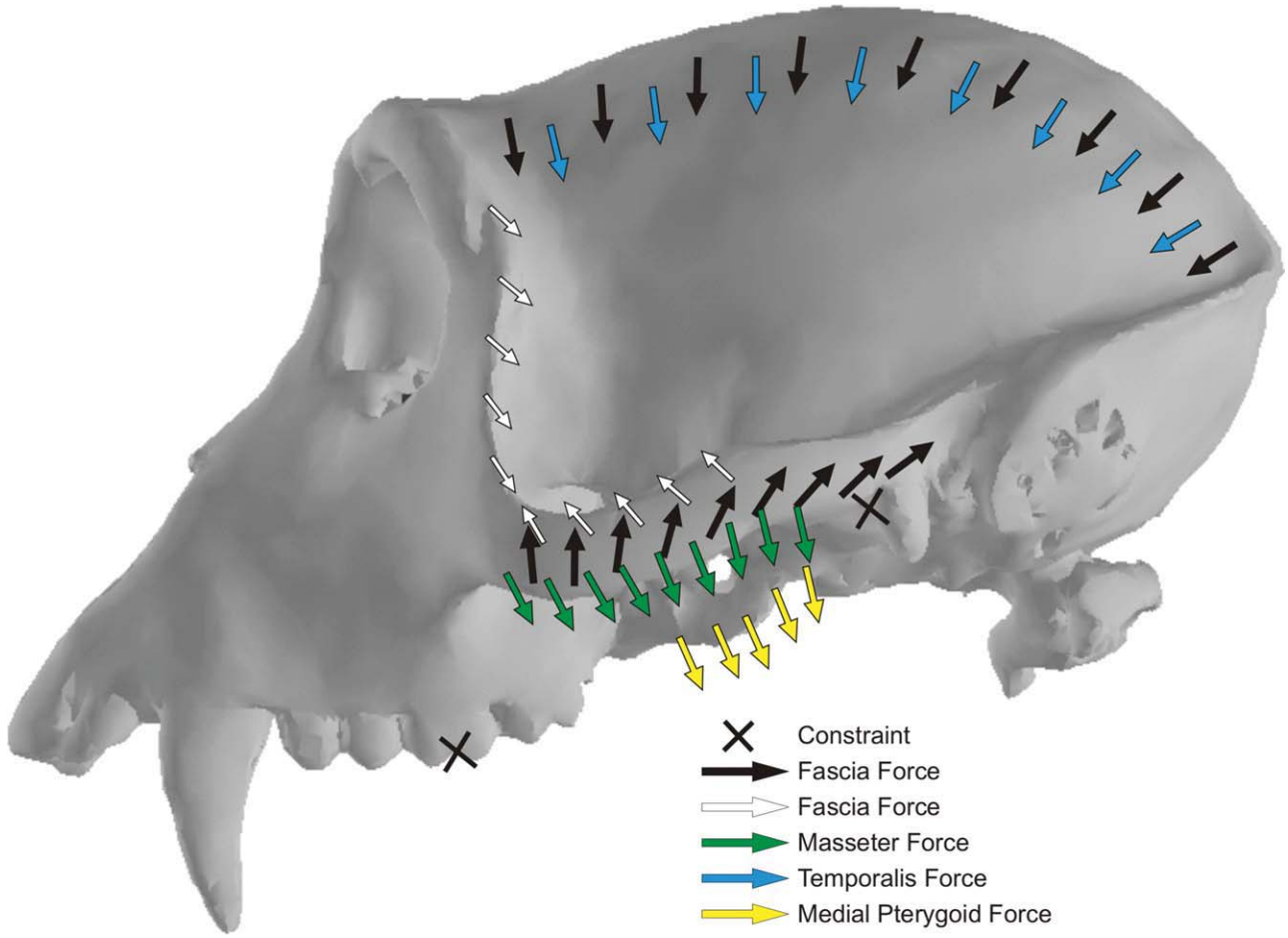

Fig. 2. Loads and constraints applied to the 3D finite element model. Note that simulations were also carried out without the fascial forces. Masseter includes superficial and deep portions.

simulated, and a solution reference temperature of zero and an expansion coefficient of 0.07 (/°C) were assigned. Note that the absolute values of the parameters assigned to the muscles are unimportant since they were iteratively varied until a representative level of muscle bulging was achieved. A muscle bulge that resulted in a peak lateral displacement of 1 mm was simulated, and the relative strain within the fascia was predicted. This bulge of 1 mm is a first approximation, subject to change when experimental measurements become available.

To estimate the force that this fascial strain would apply to the zygomatic arch a single pin-jointed spar element was defined within the finite element software. This spar element represents the end of the fascia, attached at one end to the temporalis muscle at the point at which the fascia leaves the muscle surface inferiorly, and to the superior aspect of the zygomatic arch at the other (see Fig. 1a). The element was defined with a representative cross-sectional area of 1 mm^2, and assigned a Poisson's ratio of 0.3 and a Young's modulus of 148 MPa (measured as part of this work, see "Results"). The fascial strain estimated from the muscle bulging simulation was applied to the spar element and the resultant force created on the attachment node on the zygomatic arch recorded.

A three-dimensional (3D) FEA was then carried out on the same macaque skull. The skull and loading conditions were identical to those used in a previous study (Curtis et al., 2008). In brief, cross-sectional areas of the temporalis, masseter, and pterygoid muscles (Anton, 1999, 2000: summarized in Ross et al., 2005) were multiplied by a muscle stress constant of 25 N/cm^2 (Cleuren et al., 1995) to estimate peak force magnitudes. For example, the maximum masseteric force (deep and superficial portions), which is of particular interest in this study as it attaches on the zygomatic arch, was calculated to be 66 N. These muscle forces were then applied to the skull in anatomically representative locations as straight-line vectors. The temporalis wrapped over the cranium, and contact/ wrapping forces were included in the model as determined from a multibody dynamics analysis (Curtis et al., 2008). The model was constructed from solid tetrahedral (ten node) higher order elements, which were specified with Young's modulus of 17 GPa and a Poisson's ratio of 0.3. The model was constrained in all directions at three nodes at the second molar on both sides of the skull, and vertically (y-axis in this model) at one node at each temporomandibular joint. Finite element simulations were conducted on a model with and without simulated temporal fascia on the left

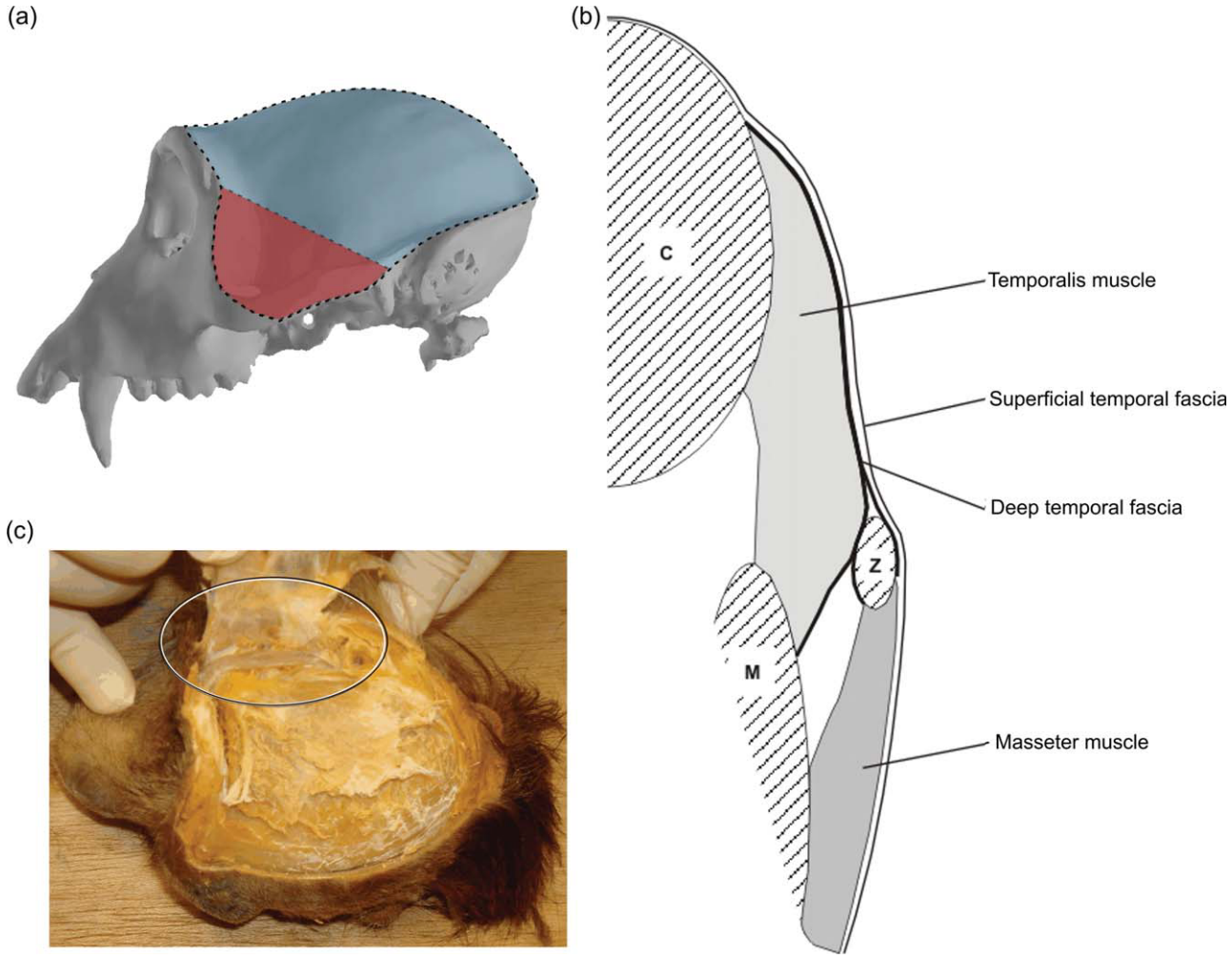

Fig. 3. Dissection findings. **a**: The deep temporal fascia in the macaque, the red part is more fibrous; **b**: Simple schematic of the fasciae and muscle anatomy obtained from human dissection. C = cranium, M = mandible, Z = zygomatic arch; and **c**: Strong ventral attachment of the deep temporal fascia onto the zygomatic arch in a macaque. Encircled region highlights the zygomatic arch and fascia, which is being pulled away to show ventral attachment.

TABLE 1. Young's modulus of adult male human temporal fasciae

Sample	Deep temporal fascia (MPa)	Superficial temporal fascia (MPa)
1	170	10
2	110	10
3	120	70
4	190	50
Average (± S.D.)	148 (± 39)	35 (± 30)

For explanation of the layers see Fig. 3.

side of the skull. Fascial anatomy was obtained from dissection. However, rather than include the fascia's effect by modeling muscle bulging as in the 2D case, 28 additional force vectors were applied to the model. Fourteen of these force vectors were applied to the zygomatic arch, five on the mid to ventral regions of the postorbital bar, and nine on the vault (Fig. 2). To represent some degree of muscle bulging, the vectors possessed a slight "off-vertical," lateral angulation. This angle was in the region of one degree. This approach was used in preference to modeling the muscle volumes themselves, because of the ease with which the model could be generated and the fact that the fascial forces could be more carefully specified and varied (if it had proven necessary). As a first approximation, the magnitudes of the force vectors acting on the arch were estimated from the 2D results.

RESULTS

Dissections

The temporalis muscle is covered by two distinct fascial layers. The most superficial being the superficial temporal fascia; this blends with the galea aponeurotica superiorly and inferiorly it passes over the lateral aspect of the zygomatic arch (Fig. 3b). Beneath lies the deep temporal fascia, which on dissection was noted to

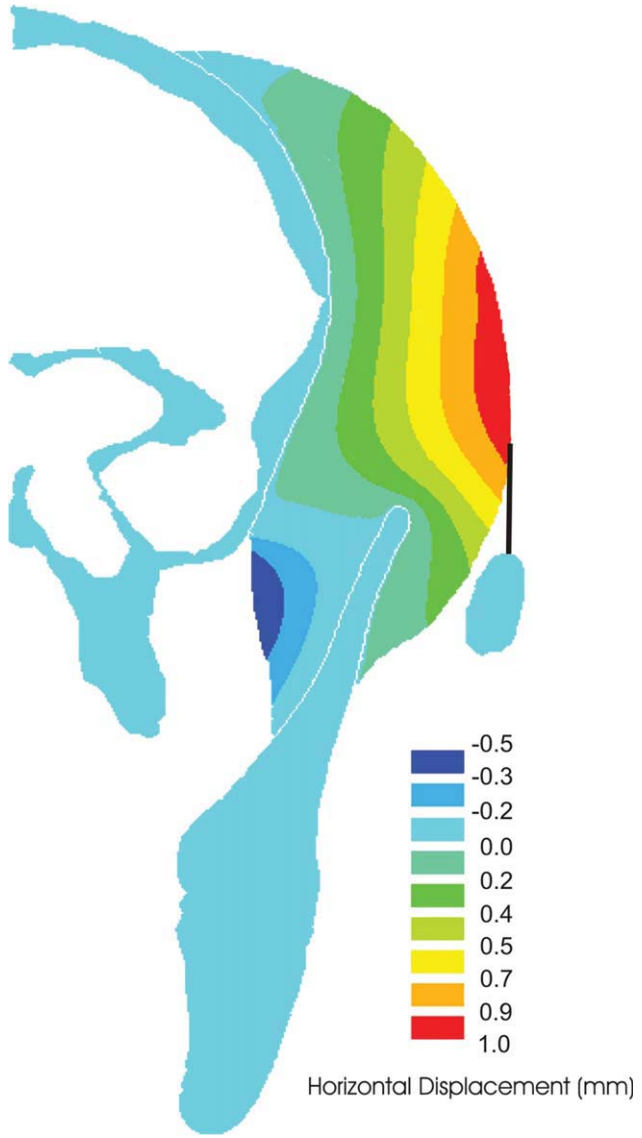

Fig. 4. Horizontal nodal displacements of the temporalis muscle during a 2D muscle bulging simulation. Simulated muscle bulge of 1 mm.

be a dense aponeurotic layer (particularly anterior; see Fig. 3a) that attaches firmly in the circumorbital region and to the zygomatic region below after splitting to encompass it. The attachment of this deep temporal fascia begins at the dorsal aspect of the zygomatic arch, where it is relatively weak and can be physically removed without additional tools. The attachment on the lateral surface is continuous over the arch. The more ventral the attachment, the more strongly it adheres to the surface of the bone, with the strongest attachment noted at the most ventral position (see Fig. 3b,c). Here, the attachment is so strong that removal of the fascia was only possible with the aid of a knife. This description of fascial attachment onto the arch agrees with Wormald and Alun-Jones (1991). It is this deep temporal fascia that was modeled in the finite element simulations.

Material Testing

Table 1 presents the material testing results of the deep temporal fascia and the superficial temporal fascia. Over all samples tested the deep temporal fascia had a mean Young's modulus of 148 MPa (± 39 MPa) and the superficial temporal fascia had a mean Young's modulus of 35 MPa (± 30 MPa). The values for the superficial temporal fascia are presented here for information; however, only the deep temporal fascia was simulated throughout this study. All samples were strained in the direction of fiber orientation.

Finite Element Analysis

The aim of the 2D FEA was to estimate the relative lengthening of the deep temporal fascia as the temporalis muscle bulges during contraction, and to predict the potential force this lengthening would apply to the zygomatic arch. A Young's modulus of 148 MPa was assigned to the fascial element during the 2D simulations, a mean value obtained for the deep temporal fascia from the experimental testing (Table 1). The simulations revealed that a temporalis bulge of 1 mm would elongate the fascia by 1.3 mm, equivalent to a strain of 3.5%. When an equivalent strain was applied to the spar element, it produced a vertical force of 3.33 N/mm (Fig. 4 presents a muscle bulging nodal displacement plot). With an effective zygomatic arch length of 27.5 mm (measured from the CT data of this specimen of *Macaca fascicularis*), this equates to an applied fascial force of 91.6 N. This force is 39% larger than the masseteric force (estimated to be 66 N), suggesting our initial simulated muscle bulge of 1 mm was too great. It was estimated that a muscle bulge of ~0.7 mm would provide a resultant force that balances the masseter muscle during forceful biting.

Thus, as a first approximation, the fascia was represented by a combined force of 66 N acting vertically along the zygomatic arch during the 3D FEA. Initial simulations indicated that a force of this magnitude caused some superior bending of the arch. In consequence, the fascial force vectors were modified until maximum (tensile) principal strains within the zygomatic arch were relatively uniform along its length. This would represent a balanced state between the pull of the masseter and the pull of the fascia. To achieve this required a total fascial force of 56 N. The original, undeformed FE model, and the model after loading are shown in Fig. 5. Here, with the deformations of the skull exaggerated (by a factor of 1,000), it is clear that the fascia, which is modeled on the left side only, significantly reduces lateral, inferior bending of the zygomatic arch as expected. Figs. 6 and 7 show the variations in maximum (tensile) principal strain and minimum (compressive) principal strain in the model with fascia modeled only on the left side of the skull. The effect is significant reductions in strains over the temporal, zygomatic, and frontal bones.

Figure 8 also shows the variations in maximum (tensile) principal strains through two cross-sections of the skull. When no fascia is modeled, there are high strain gradients along the length and through the thickness of the zygomatic arch and frontal bone. With full fascia, as simulated here, the peak strains and strain gradients

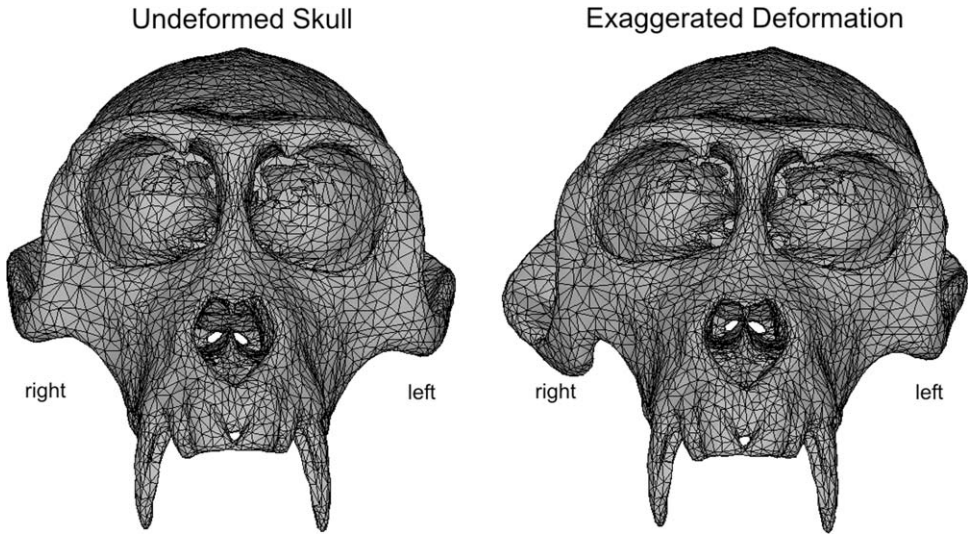

Fig. 5. The 3D finite element model showing the original, undeformed skull and the skull after loading in which deformations have been exaggerated by 1000. Fascia was modeled on the left side only.

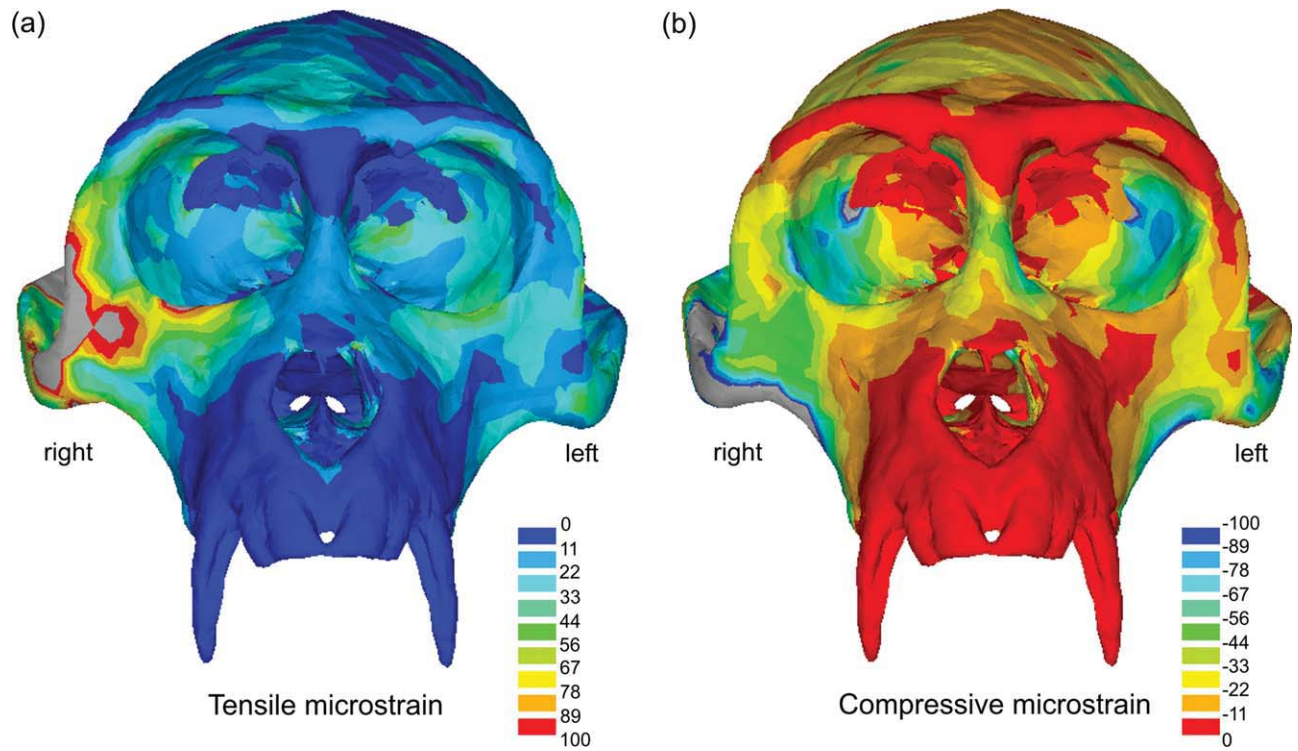

Fig. 6. Frontal view: **a**: Maximum (tensile) principal strain plot and **b**: minimum (compressive) principal strain plot. Fascia modeled on the left side only. Grey areas are in excess of 100 microstrain.

are reduced throughout, so that both the external surfaces and internal bone experience comparable levels of strain.

For comparison with *in vivo* strain gauge data, strain magnitudes were extracted at select locations on the skull (see Fig. 9). These locations were representative of strain gauge locations placed during *in vivo* testing (data presented in Ross et al., 2005; Strait et al., 2005, 2007: pooled from Hylander et al., 1991; Hylander and Johnson, 1997; Ross, 2001; Ross et al., 2002). The pooled *in vivo* strain gauge data were collected for *Macaca mulatta* and *Macaca fascicularis* and presented here as grand mean shear strains (as in Ross et al., 2005; Strait et al., 2005, 2007). Shear strains over several elements

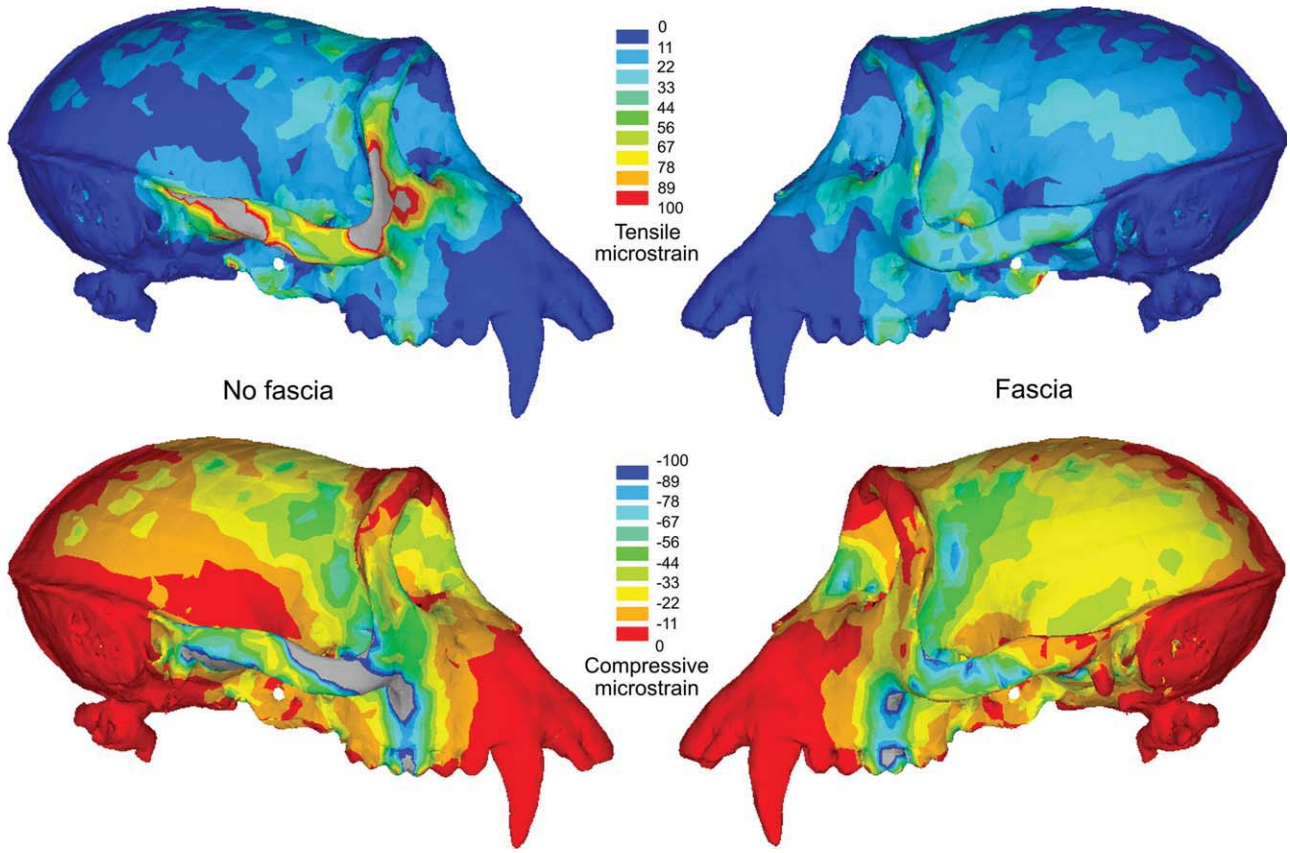

Fig. 7. Lateral view: Maximum (tensile) principal strain and minimum (compressive) principal strain plots with and without a modeled fascia. Gray areas are in excess of 100 microstrain.

were extracted, of which the mean is presented (white circles in Fig. 9 are representative of the areas from which element strains were extracted). The strain data are presented in a comparable manner to previous publications, but it should be noted that the joined points in the figures (i.e., the trend curves) are not directly related to one another. At Positions 1, 2, and 5 the average of seven elements was taken, whereas at all other positions the average of six elements was taken. The masseteric force applied in our simulations was estimated from *Macaca fascicularis* muscle data; however, the *in vivo* data used for comparison were pooled from *Macaca mulatta*, which has larger muscles, and *Macaca fascicularis*. The muscle stress value of 25 N/cm^2 we used in our muscle force calculations may be considered conservative, with others applying values closer to 40 N/cm^2 (e.g., Weijs and Hillen, 1985; Langenbach and Hannam, 1999; Sellers and Crompton, 2004). We therefore present a range of predicted strains resulting from maximum and minimum possible muscle forces, see Fig. 10.

Although maximum strain values closely matched the *in vivo* data, the average FEA shear strain predictions without temporal fascia modeled were generally lower than is found *in vivo* (Fig. 10a). The *in vivo* and FEA strain trends were however similar, indicating that the FE model deformed in similar ways to the real skull, albeit by a slightly smaller amount. Shear strains in the infraorbital and mid zygomatic arch regions, and to a lesser extent the postorbital bar (Positions 3, 4, and 5 in Fig. 10a) were considerably larger than the dorsal interorbital and dorsal orbital regions of the skull (Positions 1 and 2 in Fig. 10a).

With fascia modeled, strains in the infraorbital, mid zygomatic arch, and postorbital bar regions of the skull were reduced substantially, although shear strains in the mid zygomatic arch were still in excess of all other regions of the skull (Fig. 10b). An analysis of the maximum (tensile) and minimum (compressive) principal strains showed tensile strains to be relatively uniform at all locations of the skull, while compressive strains peaked at the mid zygomatic arch region, see Fig. 11.

DISCUSSION

Here, through computational FEAs, we assess the impact of modeling the temporal fasciae in the primate skull. The motivation for this study was provided by experimental evidence that the temporal fasciae play an important stabilising role in Cebus monkeys (Eisenberg and Brodie, 1965) and by circumstantial and clinical evidence regarding the apparent stability of isolated zygomatic arch fractures in humans (Fujii and Yamashiro, 1983; Werner et al., 2002; Turan et al., 2004; Rodriguez-Vegas and Casado Perez, 2004). Computational FEAs that aim to understand the mechanical performance of mammalian skulls rarely include these fascial structures (e.g., Ross et al., 2005; Kupczik et al., 2007, 2009; Strait et al., 2007, 2009; Wroe et al., 2007, 2010; Curtis et al.,

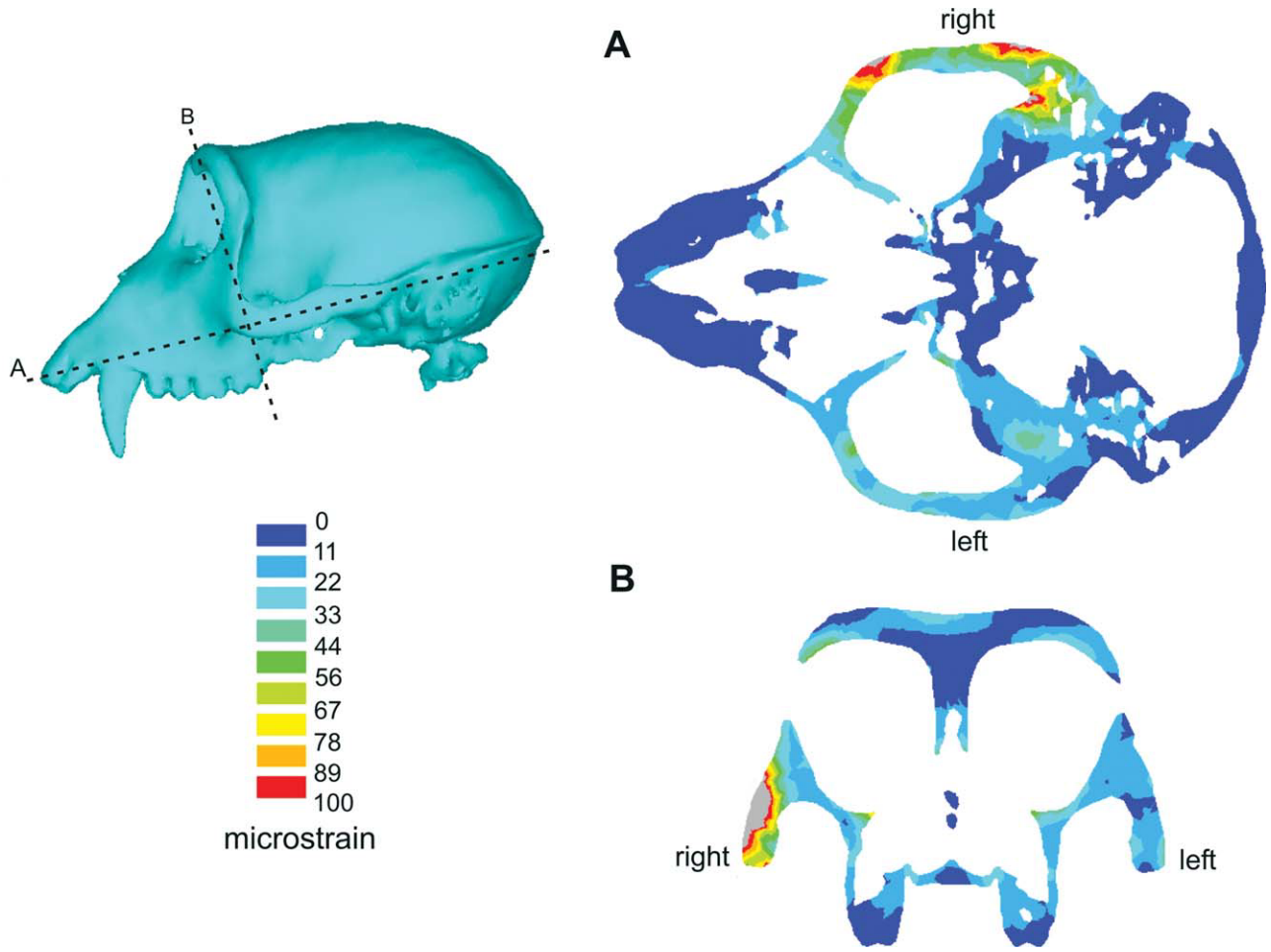

Fig. 8. Maximum (tensile) cross-sectional principal strain plots. Section A – dorsal view: Section B – frontal view. Fascia modeled on the left side only. Gray areas are in excess of 100 microstrain.

2008; Dumont et al., 2010; Wang et al., 2010), and generally report large inferior bending of the zygomatic arch and high strain gradients across the skull. When we include a complete deep temporal fascia into our FE model of a macaque skull we note a considerable reduction in peak strains, resulting in a more uniform distribution of strains across the entire zygomatic arch (Figs. 6 and 7). Large strain gradients throughout the arch and within neighboring structures were reduced not only on the surface of the skull, but throughout the entire structure, as highlighted in the cross-sectional images presented in Fig. 8.

In primates, experimental strain gauging does however show relatively high strains around the zygomatic arch and surrounding areas, with low strains in other regions of the skull (e.g., Hylander et al., 1991; Hylander and Johnson, 1997; Ravosa et al., 2000; Ross, 2001). Previous FEAs of primate skulls (e.g., Ross et al., 2005; Strait et al., 2005) agree with these *in vivo* findings, indicating significant inferior bending and twisting within the (unsupported) zygomatic arch, which also impacts on other regions of the skull (e.g., regions of the frontal and zygomatic bones). From our analyses, we note that predicted strains without a modeled fascia best match strains reported *in vivo,* with this correlation between the experimentally recorded strains and those predicted through FEA suggesting that the temporal fasciae may not aid the zygomatic arch in resisting the tensions of the masseter muscle, as previously suggested.

Although difficult to test, one possible explanation for high strain gradients recorded *in vivo* by gauges is related to the experimental procedures used to site these gauges. In removing periosteum and the overlying tissues to site the gauges there is likely to be some modification to normal physiological function. The deep temporal fascia that covers and attaches to the external surface of the zygomatic arch (see Fig. 3) will unavoidably be compromized to some degree. This is particularly likely if more than one gauge is placed onto the arch, as in Hylander and Johnson (1997). Furthermore, we have shown that the fascia inserting on the anterior aspect of the arch is thicker and will likely offer relatively greater stabilisation against bending stresses. Thus, strain gauges placed in this region are especially likely to affect the fascia's mechanical function. Both mechanical and sensory (pain or feedback) function may be affected, which could impact on the activity within the muscles and strains in several regions of the skull. Further systematic studies are required to identify whether these effects are significant.

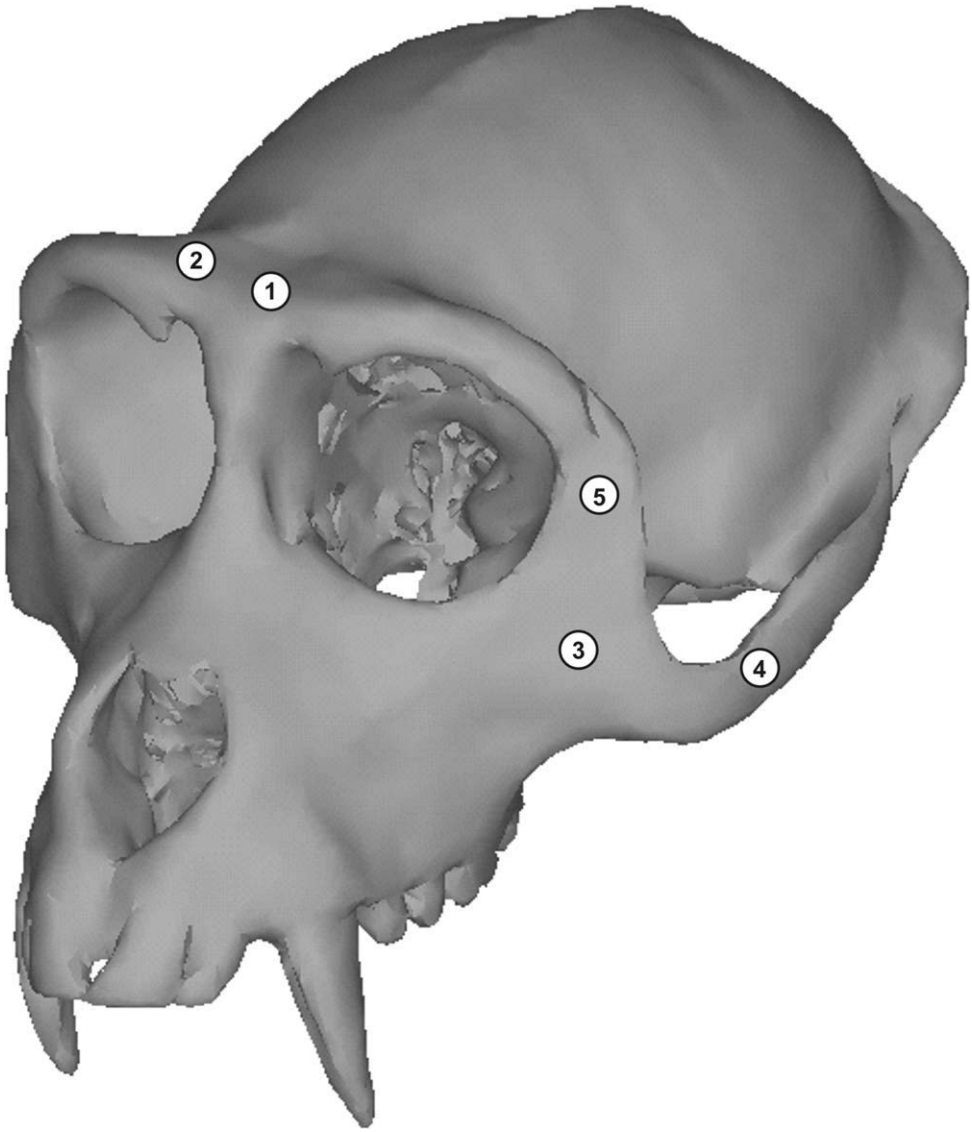

Fig. 9. Locations on the skull from which strain magnitudes were extracted. Regions: 1 - dorsal interorbital; 2 - dorsal orbital; 3 - infraorbital; 4 – mid zygomatic arch; and 5 - postorbital bar.

Our FE simulations in which no fasciae were modeled showed similar shear strains and strain trends to those of past studies (Ross et al., 2005; Strait et al., 2005, 2007 – see Fig. 10a). However, when a full deep temporal fascia was modeled there was considerable reduction in peak strains, resulting in a more uniform distribution across the entire zygomatic arch (Fig. 7). Large strain gradients throughout the arch and within neighboring structures were reduced, although shear strains were still elevated within the mid zygomatic arch region compared with other regions of the skull (Figs. 10b and 11). The arch was however free of large tensile strains associated with inferior bending and twisting (Fig. 11). Higher shear strains (linked mostly with higher compressive principal strains) in the mid zygomatic arch region are likely attributable to an imbalance between the direction of the applied masseteric and temporal fascial forces within this modeling study. In the frontal view, the masseteric forces are directed ventrally and medially, which when opposed by the almost vertical fascial forces effectively "buckle" the arch, resulting in the elevated compressive strains on its lateral surface (as shown in Figs 7 and 11). Thus, this finding may be in part attributable to modeling approximations, most notably the estimated lines-of-action of the force vectors and possibly the omission of the zygomaticotemporal suture.

Here, we model masseteric forces as straight-line vectors applied in the direction defined from approximate origin and insertion locations on the cranium and mandible, respectively. As the masseter muscle contracts, it will also bulge, which will modify its force line-of-action, shifting it laterally with respect to the midline; this will reduce the resultant medial force component that exists between the masseter and temporal fascia vectors. Coinciding with this masseteric bulging is bulging of the temporalis muscle, which may direct the deep temporal

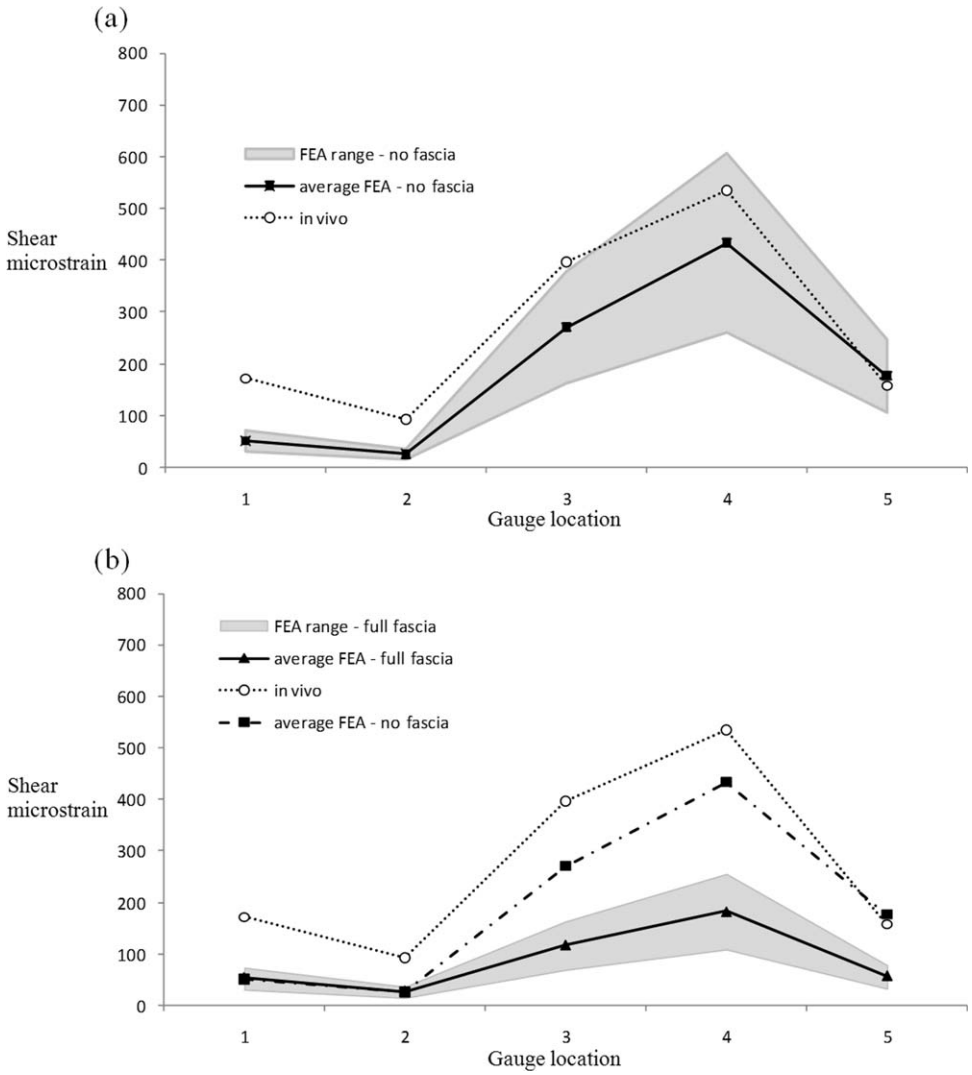

Fig. 10. In vivo, range of FEA, and mean FEA shear strains at: 1 - dorsal interorbital; 2 - dorsal orbital; 3 - infraorbital; 4 – mid zygomatic arch; and 5 - postorbital bar regions of the skull. Range of FEA includes upper and lower strain limits caused by upper and lower possible muscles forces. **a**: No fascia modeled and **b**: full fascia modeled.

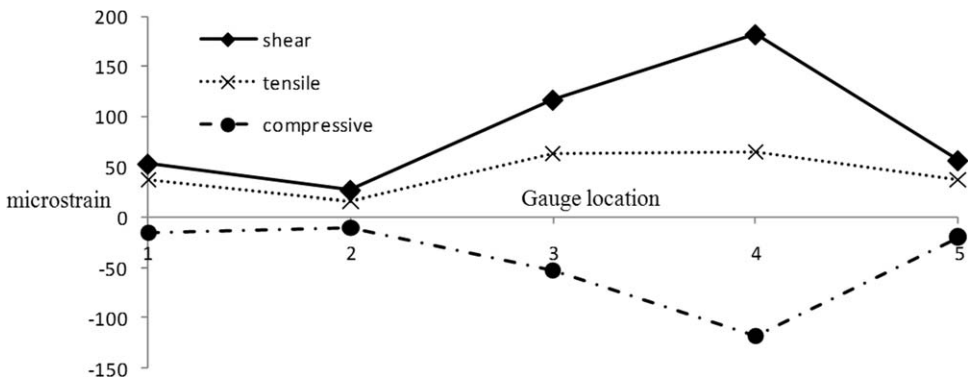

Fig. 11. Mean FEA tensile, compressive, and shear strains over the skull with a modeled temporal fascia: 1 - dorsal interorbital; 2 - dorsal orbital; 3 - infraorbital; 4 – mid zygomatic arch; and 5 - postorbital bar regions of the skull.

fascia force vectors more laterally than is simulated in this study, further reducing the resultant medial force component that exists between the masseter and temporal fascia. Some medial force component is likely to exist however, as the vaulted zygomatic arch will, to some extent, resist this force. Medial displacement of bone fragments in isolated zygomatic arch fractures in humans also suggests some medial force component exists (e.g., Özyazgan et al., 2007; Yamamoto et al, 2007).

The 2D FEA revealed that minimal muscle bulging (0.7 mm) could generate enough force within the facia to equal that of the masseter muscle. The degree of muscle bulging necessary is of course sensitive to the material properties assigned to the fascia. Here we used experimentally measured values from a human specimen in order to obtain a first approximation, but this value may differ in other primates. A more or less stiff material will require less or more (respectively) muscle bulging to generate sufficient forces to balance those of the masseter muscle. We simulated only deep temporal fascia, ignoring any contribution of the superficial temporal fascia because its anatomy suggests it plays little if any role in stabilising the zygomatic arch. In the 3D FEA, a total fascial force lower than that found in the 2D simulation produced a near bending-free situation (or at least a situation free of inferior bending and twisting associated with the unsupported arch) within the zygomatic arch. Fascial forces equivalent to 85% of the magnitude of masseteric forces (56 N and 66 N, respectively) satisfied this criterion. There are of course several approximations and assumptions that impact on the findings of this study. Muscle forces, material properties of the bone and fascia, and representations of the fascia in the 2D and 3D simulations are all approximations that are subject to refinement as experimental data become available. However, this does not affect the overall focus and conclusions of this study that the temporal fasciae could aid the zygomatic arch in resisting the tensions of the masseter.

To summarize, through computational FEAs we have shown the temporal fasciae that attach to the zygomatic arch in primates and most other mammals could add significant stabilisation to the arch against the forceful downward loads applied by the masseter muscle during biting. Removal of the fasciae results in elevated strains that could explain the bone adaptation recorded in past experimental studies. This raises an issue of some importance to future modeling studies of craniofacial strains not only in primates, but potentially in all other skulls where fasciae and/ or other soft tissue (or even more ossified) structures exist.

ACKNOWLEDGEMENT

The authors would like to thank Callum Ross (University of Chicago, USA) for his constructive comments on an earlier draft of this manuscript.

LITERATURE CITED

Al Dayeh AA, Rafferty KL, Egbert M, Herring SW. 2009. Deformation of nasal septal cartilage during mastication. J Morph 279:1209–1218.

Anton SC. 1999. Macaque masseter muscle: internal architecture, fiber length, and cross-sectional area. Int J Prim 20:441–462.

Anton SC. 2000. Macaque pterygoid muscles: internal architecture, fiber length, and cross-sectional area. Inter J Prim 21:131–156.

Brodie GA. 1952. Consideration of musculature in diagnosis, treatment and retention. Am J Ortho 38:823–835.

Cleuren J, Aerts P, De Vree F. 1995. Bite and joint force analysis in *Caiman crocodilus*. Belg J Zool 125:79–94.

Currey JD. 2002. Bones: structure and mechanics. Princeton and Oxford: Princeton University Press.

Currey JD. 2005. Bone architecture and fracture. Curr Osteoporos Rep 3:52–56.

Curtis N, Kupczik K, O'Higgins P, Moazen M, Fagan MJ. 2008. Predicting skull loading: applying multibody dynamics analysis to a macaque skull. Anat Rec 291:491–501.

Dumont ER, Davis JL, Grosse IR, Burrows AM. 2010. Finite element analysis of performance in the skulls of marmosets and tamarins. J Anat. Available online - doi: 10.1111/j.1469–7580.2010.01247.x.

Dumont ER, Grosse IR, Slater GJ. 2009. Requirements for comparing the performance of finite element models of biological structures. J Theor Biol 256:96–103.

Eisenberg NA, Brodie AG. 1965. Antagonism of temporal fascia to masseteric contraction. Anat Rec 152:185–192.

Fujii N, Yamashiro M. 1983. Classification of malar complex fractures using computed tomography. J Oral Maxillofac Surg 41:562–567.

Holmes HG. 1912. Case of absence of the zygomatic arch. Australus M Gaz Sydney 31:247.

Hylander WL, Johnson KR. 1997. In vivo strain patterns in the zygomatic arch of macaques and the significance of these patterns for functional interpretations of craniofacial form. Am J Phys Anthro 102:203–232.

Hylander WL, Picq PG, Johnson KR. 1991. Masticatory-stress hypotheses and the supraorbital region of primates. Am J Phys Anthro 86:1–36.

Kupczik K, Dobson CA, Crompton RH, Phillips R, Oxnard CE, Fagan MJ, O'Higgins P. 2009. Masticatory loading and bone adaptation in the supraorbital torus of developing macaques. Am J Phys Anthro 139:193–203.

Kupczik K, Dobson CA, Fagan MJ, Crompton RH, Oxnard CE, O'Higgins P. 2007. Assessing mechanical function of the zygomatic region in macaques: validation and sensitivity testing of finite element models. J Anat 210:41–53.

Langenbach GEJ, Hannam AG. 1999. The role of passive muscle tensions in a three-dimensional dynamic model of the human jaw. Arch Oral Biol 44:557–573.

Moore WJ. 1967. Muscular function and skull growth in the laboratory rat (Rattus norvegicus). J Zool Lond 152:287–296.

Moss ML, Salentijn L. 1969. The capsular matrix. Am J Orthod 56:474–490.

Oxnard CE, Franklin D. 2008. Ghosts of the past I: Some muscles and fasciae in the head domain. Folia Primatol 79:429–440.

Özyazgan I, Günay GK, Eskitaşçıoğlu T, Özköse M, Çoruh A. 2007. A new proposal of classification of zygomatic arch fractures. J Oral Maxillofac Surg 65:462–469.

Preuschoft H, Witzel U. 2002. Biomechnical investigations on the skulls of reptiles and mammals. Senckenbergiana Lethaea 82:207–222.

Ravosa MJ, Noble VE, Hylander WL, Johnson KR, Kowalski EM. 2000. Masticatory stress, orbital orientation and the evolution of the primate postorbital bar. J Hum Evol 38:667–693.

Rodriguez-Vegas JM, Casado Perez C. 2004. Inexpensive custom-made external splint for isolated closed zygomatic arch fractures. Plast Reconstr Surg 113:1517–1518.

Ross CF. 2001. In vivo function of the craniofacial haft: the interorbital "pillar". Am J Phys Anthropol 116:108–139.

Ross CF, Patel BA, Slice DE, Strait DS, Dechow PC, Richmond BG, Spencer MA. 2005. Modeling masticatory muscle force in finite element analysis: sensitivity analysis using principal coordinates analysis. Anat Rec 283:288–299.

Ross CF, Strait DS, Richmond BG, Spencer MA. 2002. In vivo bone strain and finite-element modeling of the anterior root of the zygoma of *Macaca*. Am J Phys Anthropol 34 (Suppl.):133.

Sellers WI, Crompton RH. 2004. Using sensitivity analysis to validate the predictions of a biomechanical model of bite forces. Ann Anat 186:89–95.

Shira RB. 1981. An architectural and structural craniofacial analysis: a new lateral cephalometric analysis. Oral Surg 52:226–238.

Strait DS, Richmond BG, Spencer MA, Ross CF, Dechow PC, Wood BA. 2007. Masticatory biomechanics and its relevance to early hominid phylogeny: an examination of palatal thickness using finite element analysis. J Hum Evol 52:585–599.

Strait DS, Wang Q, Dechow PC, Ross CF, Richmond BG, Spencer MA, Patel BA. 2005. Modeling elastic properties in finite element analysis: how much precision is needed to produce an accurate model? Anat Rec 283:275–287.

Strait DS, Weber GW, Neubauer S, Chalk J, Richmond BG, Lucas PW, Spencer MA, Schrein C, Dechow PC, Ross CF, Grosse IR, Wright BW, Constantino P, Wood BA, Lawn B, Hylander WL, Wang Q, Byron C, Slice DE, Smith AL. 2009. The feeding biomechanics and dietary ecology of *Australopithecus africanus*. PNAS 106:2124–2129.

Turan A, Kul Z, Haspolat Y, Işler C, Ozsoy Z. 2004. Use of tracheal tube in isolated fractures of the zygomatic arch. Plast Reconstr Surg 114:1005–1006.

Wang Q, Wright BW, Smith A, Chalk J, Byron CD. 2010. Mechanical impact of incisor loading on the primate midfacial skeleton and its relevance to human evolution. Anat Rec 293:607–617.

Weijs WA, Hillen B. 1985. Cross-sectional areas and estimated intrinsic strength of the jaw muscles. Acta morph Neerl scand 23:267–274.

Werner JA, Frenkler JE, Lippert BM, Folz BJ. 2002. Isolated zygomatic arch fracture: report on a modified surgical technique. Plast Reconstr Surg 109:1085–1089.

Witzel U, Mannhardt J, Goessling R, De Micheli P, Preuschoft H. 2011. Finite element analyses and virtual syntheses of biological structures and their application to sauropod skulls. In: Klein N, Remes K, Gee CT, Sander PM, editors. Biology of the sauropod dinosaurs: understanding the life of giants. Bloomington: Indiana University Press, Chapter 10, 171–181.

Witzel U, Preuschoft H. 2005. Finite-element model construction for the virtual synthesis of the skulls in vertebrates: case study of *Diplodocus*. Anat Rec 283:391–401.

Witzel U, Preuschoft H, Sick H. 2004. The role of the zygomatic arch in the statics of the skull and its adaptive shape. Folia Primatol 75:202–218.

Wormald PJ, Alun-Jones T. 1991. Anatomy of the temporal fascia. J Lary Otol 105:522–524.

Wroe S, Ferrara TL, McHenry CR, Curnoe D, Chamoli U. 2010. The craniomandibular mechanics of being human. Proc R Soc B 277:3579–3586.

Wroe S, Moreno K, Clausen P, McHenry CR, Curnoe D. 2007. High-resolution three-dimensional computer simulation of hominid cranial mechanics. Anat Rec 290:1248–1255.

Yamamoto K, Murakami K, Sugiura T, Fujimoto M, Inoue M, Kawakami M, Ohgi K, Kirita T. 2007. Clinical analysis of isolated zygomatic arch fractures. J Oral Maxillofac Surg 65:457–461.